



A combination of 3D printing and PCB technologies in microfluidic sensing device fabrication

Hang Tran Thanh¹ · Tuan Vu Quoc^{1,2} · Phu Nguyen Van³ · Loc Do Quang³ · An Nguyen Ngoc¹ · Chi Tran Nhu¹ · Nam Nguyen Hoang³ · Ngoc Thanh Le^{4,5} · Tran Thuy Nguyen^{4,5} · Tung Thanh Bui¹ · Trinh Chu Duc¹

Received: 2 June 2021 / Accepted: 22 March 2022 / Published online: 12 May 2022
© The Author(s), under exclusive licence to Springer-Verlag GmbH Germany, part of Springer Nature 2022

Abstract

Microfluidic devices are increasingly being used as analytical systems, biomedical devices, chemistry and biochemistry instruments, and basic research systems. Fabrication of microfluidic devices using 3D printing and PCB technologies provides faster, less expensive routes to devices than the microelectronics-derived method. Since cleanroom is not a compulsory requirement and the entire fabrication process can be done in only one day, the proposed approach is more accessible to chemists and biologists working under benchtop conditions. In this work, the replica molding based on 3D printing for microfluidic channel realization and low-cost PCB manufacturing process for microelectrode structure formation were combined to apply in microfluidic device fabrication. Obtained results show that microfluidic channel structures can be fabricated with a success rate of up to 80% for the case of the 200- μm -in-dimension channel. Besides, a microfluidic lab-on-chip device capable of generating and sensing microdroplets was implemented to validate the usability of the proposed fabrication process. With the fabricated devices, microdroplets with sizes varying from 100 to 310 nL were successfully formed and detected based on the fluidic flow impedance detection technique. These results demonstrate that the combination of 3D printing and PCB technologies is a good option for the rapid prototyping of microfluidic devices aimed at complicating lab-on-a-chip (LoC) systems.

1 Introduction

Medicine, chemical, and biological fields are the topics that attract many researchers (Ashraf et al. 2020a, b, c). Microfluidics is becoming more significant in that wide range of these applications (Han and Chen 2020; Lv et al. 2022; Rahman and Rebrov 2014; Rapp et al. 2010). The decrease in size, weight, and power consumption; enhancement insensitivity; and low-cost batch production properties of these devices have made the technology particularly desirable for various applications, e.g., microarrays, micromixers, DNA sequencing, sample preparation and analysis, cell separation and detection, and environmental monitoring, just to name a few (Lv and Chen 2021; Lv et al. 2021; Tran et al. 2021; Vu-Dinh et al. 2021). These microfluidic devices have shown considerable promise in terms of lowering manufacturing costs, reagent use, analysis time, and increasing device efficiency and mobility (Scott and Ali 2021).

Because of the micron diameter channel of the microfluidic system, numerous traditional manufacturing

✉ Tuan Vu Quoc
vqtuan0211@capsi.vast.vn

✉ Trinh Chu Duc
trinhcd@vnu.edu.vn

Loc Do Quang
locdq@vnu.edu.vn

¹ University of Engineering and Technology, Vietnam National University, Hanoi, Vietnam

² Institute of Physics, Vietnam Academy of Science and Technology, Hanoi, Vietnam

³ University of Science, Vietnam National University, Hanoi, Vietnam

⁴ University of Medicine and Pharmacy, Vietnam National University, Hanoi, Vietnam

⁵ Cardiovascular Center, E Hospital, Hanoi, Vietnam

processes have been used to create microfluidic structures. Photolithography is a high-end technology that is commonly used to create the master mold for microfluidic channel creation (Quang et al. 2019, 2020; Vu-Dinh et al. 2021). Though the process can create a high-precision structure, it necessitates several fabrication procedures, a clean room, and highly accurate machining, resulting in high operating costs and a lengthy fabrication time. Rapid manufacturing at a low cost is critical for constructing extremely advanced lab-on-a-chip (LoC) devices that have the potential to change healthcare, biology, chemistry, and other areas. However, such progress may be hampered by expensive and restricted fabrication facilities, as well as techniques that lack upscaling potential.

Recently, the rapid prototyping technique (RPT) has been realized as an alternative to improve conventional fabrication methods using the three-dimensional (3D) additive printing process. 3D printing technology has been applied in prototyping devices in a variety of microfluidic research due to its flexibility in geometrical designs and ease in manufacturing (Bishop 2016). RPT has recently been realized as an alternative candidate to improve current manufacturing processes and utilized in many microfluidic studies.

Microfluidic devices have been created using a variety of 3D printing techniques, including inkjet 3D printers (i3DP), fused deposition modeling (FDM), stereolithography (SLA), and two-photon polymerization (2PP). Among the various 3D printing technologies, PolyJet by Stratasys stands out from the others due to the uniqueness of this technology, which allows the user to have a high-resolution part made with a wide selection of material properties (Bandyopadhyay and Heer 2018). Furthermore, this printer can be housed in a standard room without the need for a specialized laboratory environment though ventilation/air cleansing is encouraged (Yang et al. 2017).

Together with the 3D printing technology, the idea of the lab-on-printed circuit board (Lab-on-PCB) has re-emerged as a trend in an increasing number of the research reported in recent years (Moschou and Tserepi 2017). As the name suggests, microfluidics channels, sensors, and actuators can be integrated on the same PCB platform rapidly and easily at a low cost thanks to the ubiquity of PCB technologies. Kontakis et al. (2009) have introduced a polymer microchannel on top of a specific PCB-based design to determine flow rate in a microchannel. PCB technologies have also been used to integrate micro-pumps, valves, electrochemical sensors, immunosensor on a circuit board to create lab-on-a-chip (LoC) devices (Liu et al. 2008; Marshall et al. 2012; Sánchez et al. 2016). This technology has a high potential for upscaling the manufacture of microfluidic and LoCs devices (Moschou and Tserepi 2017).

This research proposes an RPT combining 3D printing and PCB technologies to solve the aforementioned challenge using a microfluidic chip as an example. This proposed approach removes the requirement of a cleanroom and expensive materials and equipment used for the conventional photolithography process. A 3D-printed master mold was employed to create a microfluidic channel structure using a soft-lithography method, while the microelectrode structure was realized by a low-cost PCB manufacturing process. The whole microfluidic chip was packaged using a thin liquid-PDMS layer to produce an insulating layer and an adhesive layer between the PDMS substrate and PCB platform. In order to verify the possibility and feasibility of the proposed method, a lab-on-PCB microfluidic platform for droplet generation and detection was designed, fabricated, and examined by the typical microfluidic actuator and sensor applications. Figure 1 depicts a lab-on-a-PCB platform combining 3D printing and PCB technique. The suggested Lab-on-PCB technology has two major components: a microfluidic channel structure substrate and a micro-electrode structure printed on board substrate. The Y-junction-shaped microfluidic channel employed a two-phase flow technique to generate microdroplets and control their size. These generated microdroplets were detected in-flow by using the three-electrode structure coupled with the differential amplifier method to sense the electrical properties of the microdroplets. A signal processing circuit was adapted to experimentally examine the functionalities of the fabricated device. The primary goal of this research was to provide a rapid prototyping approach for producing an efficient fabrication process of a microfluidic flow detecting platform.

2 Method and fabrication

The combinative technique consists of many phases as shown in Fig. 2. First, a 3D master mold is created using computer-aided design (CAD) software and a high-resolution 3D printing technology. After that, the PDMS is cast into the printed master mold. The master mold is then removed after curing, leaving a layer of PDMS embossed with the microfluidic channel design. Simultaneously, a three-electrode differential capacitive sensor is developed and manufactured on a PCB substrate. The resultant PCB substrate is coated by a thin PDMS layer on the electrode side, as the adhesion and insulation layer at the same time. The PDMS microfluidic channel structure is then attached to the coated PCB substrate by heating it for 2 h on a hot plate. Unlike conventional methods, the manufacturing process does not necessitate the use of a cleanroom. The

Fig. 1 An example of a lab-on-PCB microfluidic device combining 3D printing and PCB techniques

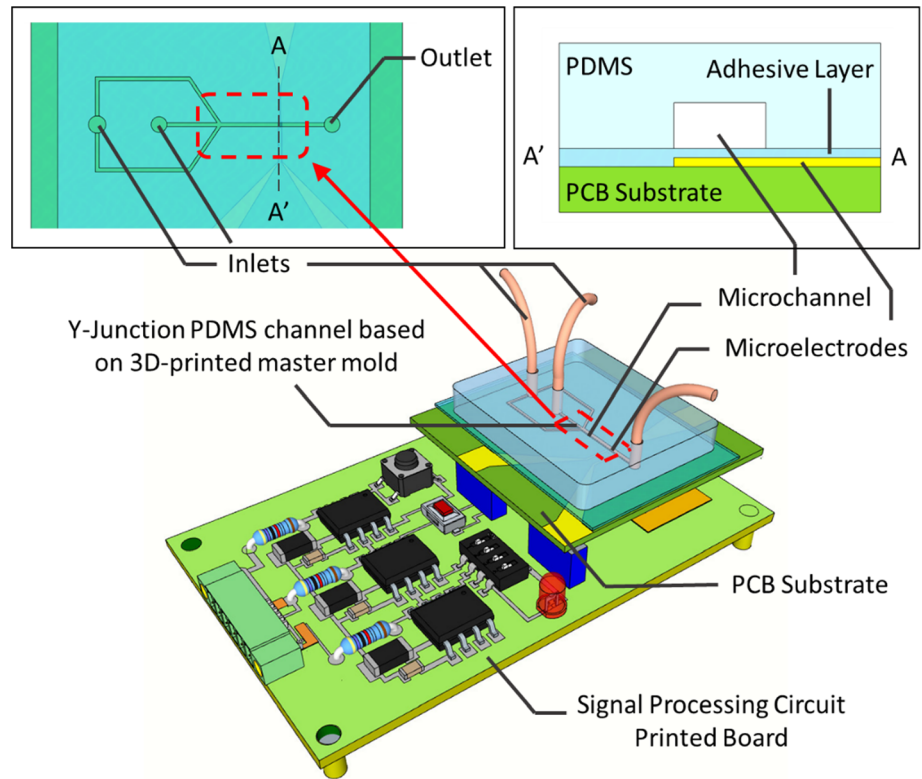
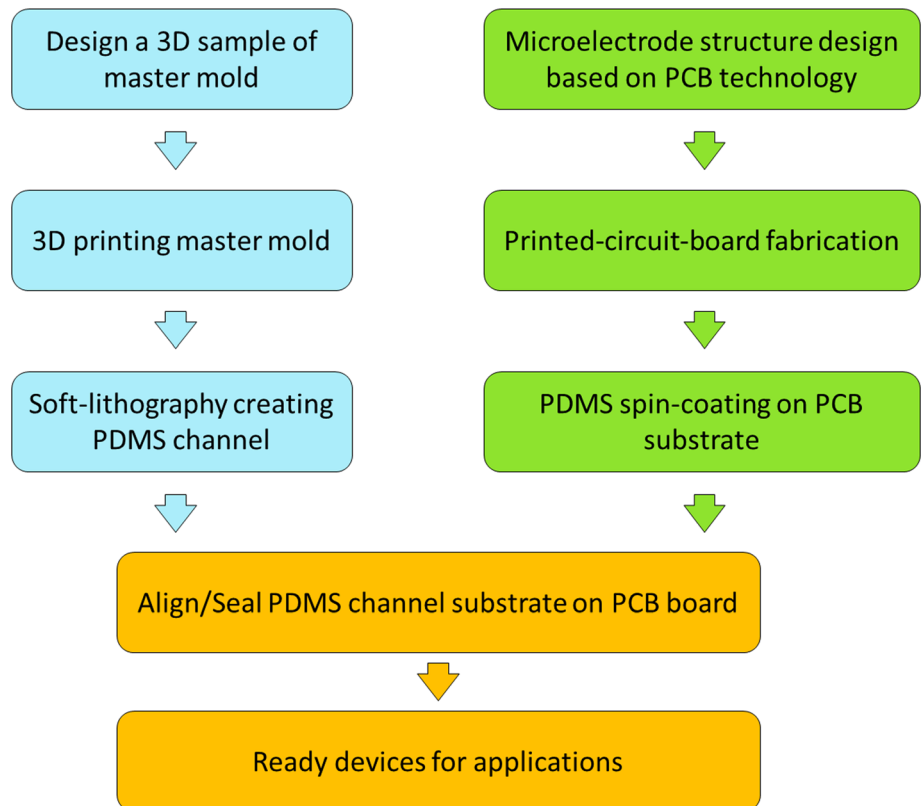


Fig. 2 Lab-on-a-chip device fabrication process based on 3D printing and PCB technologies



following sections go into further detail about each stage of the fabrication process.

2.1 Microfluidic mold preparation using 3D printing technology

The conventional microfabrication process utilizing soft-lithography technique based on a negative photoresist (e.g., SU-8) was employed as a standard for microfluidic channel formation over the past 20 years. However, this approach commonly requires the use of the master mold made by the photolithography process, which needs to be fabricated in a cleanroom and uses expensive chemicals and materials. Various efforts have been made to reduce manufacturing costs and simplify the fabrication process of the SU-8 master mold and PDMS microchannel creation (Campo and Greiner 2007; Li et al. 2008; Pinto et al. 2014). There are still several limitations in fabricating molds for microfluidic channel structures, including using reagents and equipment that are not readily available worldwide. With technological advancements in recent years, 3D printing technology has emerged as a viable alternative option for mold manufacturing with fewer strict standards, a shorter fabrication time, and a lower cost. Furthermore, the use of 3D-printed mold enables the use of commodity equipment without the need for a cleanroom and expensive materials and equipment for the standard photolithography process. Recent studies have reported on the manufacture of master molds for microfluidic channels using 3D printing methods. Kise et al. (2015) described a low-cost FDM 3D printing equipment for creating a microfluidic channel. Although the FDM 3D printing technology has a lower resolution than other approaches, it still has much potential in microfluidic creation. The SLA technology, which was employed in the high-quality fabrication of the 3D model, has been introduced to facilitate the microfabrication process (Au et al. 2015; Chen et al. 2014; Comina et al. 2014). The PDMS channels, micro-valves of fluidic channels have been created by 3D-printed master mold generation. A microfluidic mixer was directly printed to create a droplet and a whole device for biochemical synthesis and analysis. Besides, inkjet 3D printer, also one of the high-quality 3D printing technologies, has been exploited for rapid fabrication of microfluidic by printing 3D mold for PDMS microchannel (Bonyár et al. 2010; Donvito et al. 2015; Waheed et al. 2016; Walczak and Adamski 2015).

In this work, the PolyJet technology was employed to create the 3D printing master mold for the microfluidic channel. Molds are designed using computer-aided design (CAD) software. The Stratasys Objet500 Connex3 system, in particular, uses the geometric design freedoms and multi-material capability of the PolyJet 3D printing process

to create compliant mechanisms with optimal topology and high accuracy. PolyJet printing employs inkjet technology with a vertical resolution of the layer thickness of up to 14 μm deposited from a 1200 DPI nozzle. Multiple nozzles spray small droplets onto the construction area, which are then instantly exposed to UV light for each layer, resulting in great precision. However, due to the surface energy interaction between the ink and the substrate, the deposited polymer droplet will spread to a diameter different from the in-flight droplet's diameter. In the fabrication of the master mold for PDMS microchannel realization, the formation of 3D structure from the train of droplets is more complex than the patterning with a single droplet of liquid photopolymer. Several factors affect the dimension of the printed 3D structure, such as fluid properties, the rate of phase change, and the flow rate of polymer ink from the nozzle. Walczak et al. proposed a theoretical calculation of the printed line width W formed by the combination of droplets printed with defined spacing s as follows (Walczak and Adamski 2015):

$$W = SR \times d_{in-flight} \times \sqrt{\frac{2 \times \pi \times d_{in-flight}}{3 \times s \times SR^2 \times \left(\frac{\theta}{\sin^2\theta} - \cot\theta\right)}} \quad (1)$$

With SR is the spread ratio between the spread droplet diameter on the substrate d_{spread} and in-flight droplet diameter $d_{in-flight}$, and θ is the contact angle of the droplet. The complicated geometry may be maintained by a thin raft and the encasing of the portion in the support material, which is readily removed after completion. Manual peeling, WaterJet, or soaking in a sodium hydroxide (NaOH) solution can be used to remove supporting material, although NaOH has been shown to damage the gloss finish of parts (Anon 2019). The use of 3D printing technology has greatly lowered the time and expense necessary to produce microfluidic devices. Most crucially, these technologies were less expensive and required fewer rigorous criteria, allowing a broader society to adopt them. Figure 3 shows the design of the droplet generation microfluidic structure utilizing the flow-focusing approach for demonstrating the proposed rapid prototyping technique.

The design area for functionally graded materials and structures has grown dramatically as multi-material additive manufacturing technology advances. To fully utilize this feature, a thorough understanding of the interface qualities is required since they can substantially impact the overall mechanical behavior. Cazon et al. discovered that printing orientations and surface roughness substantially impacted the mechanical characteristics (Cazón et al. 2014). According to Bass et al., specimens placed

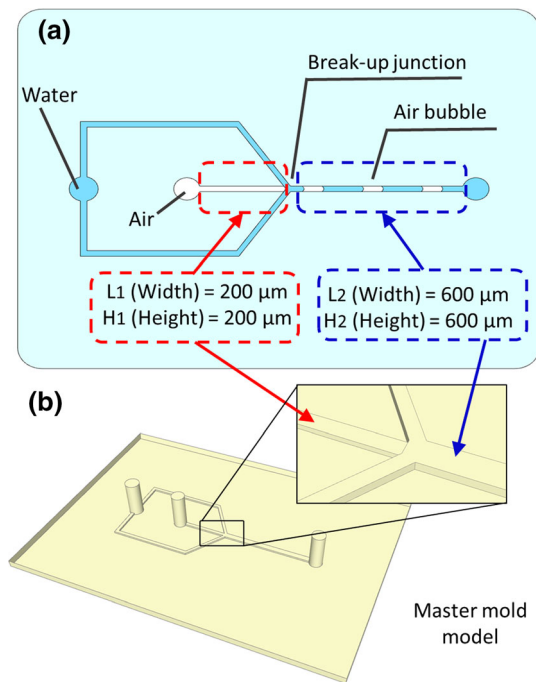


Fig. 3 Design of the Y junction flow-focusing droplet generator. **a** Structure of Y junction channels, **b** A 3D design of master mold of Y junction micro-channels

parallel to the printing direction are stronger than those oriented transversely (Bass et al. 2016). While most of the studies focused on the mechanical reactions of 3D-printed materials, understanding them from a microstructural standpoint is as important. One of the most important factors to consider when dealing with 3D-printed pieces that contain more than one material is the interface. Traditional composites have two separate boundaries that cause the composite to break at the interface layer because of delamination. Vu et al. (2018, 2020) also explored the adhesive behavior of different material layers. Failure is shown to occur most frequently at the interfaces between layers, and characteristics such as printing orientation, post-curing, and strain rate all affect the fracture resistance of the specimens.

The Stratasys Objet500 Connex3 system provides a variety of materials for the fabrication of the required model. Furthermore, the 3D-printed mold created by the proposed technique for producing microfluidic channel structures was executed using various materials, including Rigur RGD450, VeroBlue RGD840, and VeroClear RGD810. The 3D printer provides a variety of materials for the fabrication of the desired model. Rigur RGD450 was chosen among these materials due to its superior dimensional stability, greater elongation at break, greater durability, and flexibility for sub-millimeter size objects (Table 1). The master mold was retrieved from the printing bed and cleaned to remove the remaining support material

after printing with the glossy surface treatment. The master mold is removed from the printing bed, and a high-pressure water jet is used to remove any remaining support material. After that, the master mold is kept at ambient temperature and can be used many times. Figure 4 depicts the cleaned molds created from Rigur RGD450, VeroBlue RGD840, and VeroClear RGD810.

2.2 PDMS processing

The use of PDMS in microfluidic devices has been widely described (Chen et al. 2016; McDonald et al. 2000; McDonald and Whitesides 2002). The microfluidic structure was created by casting the PDMS mixture on a 3D printing master mold with the microchannel design (Fig. 5a–f).

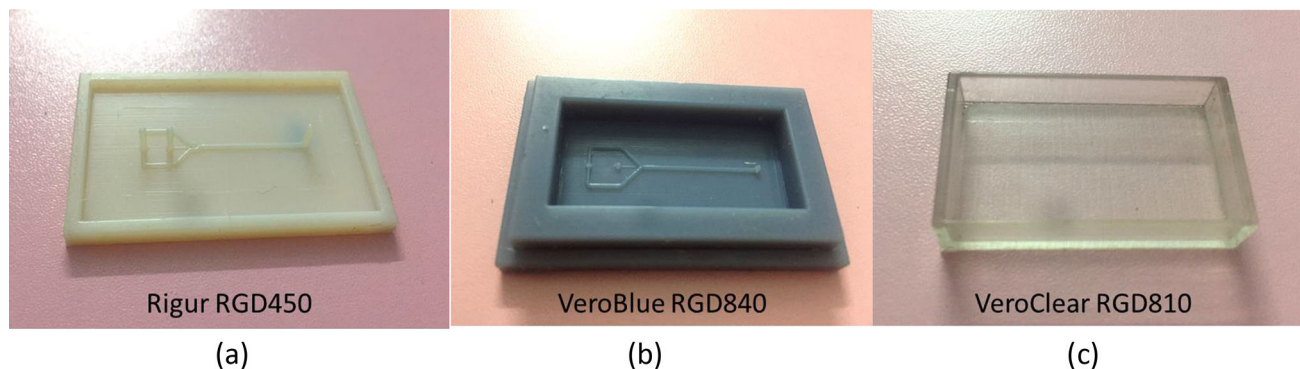
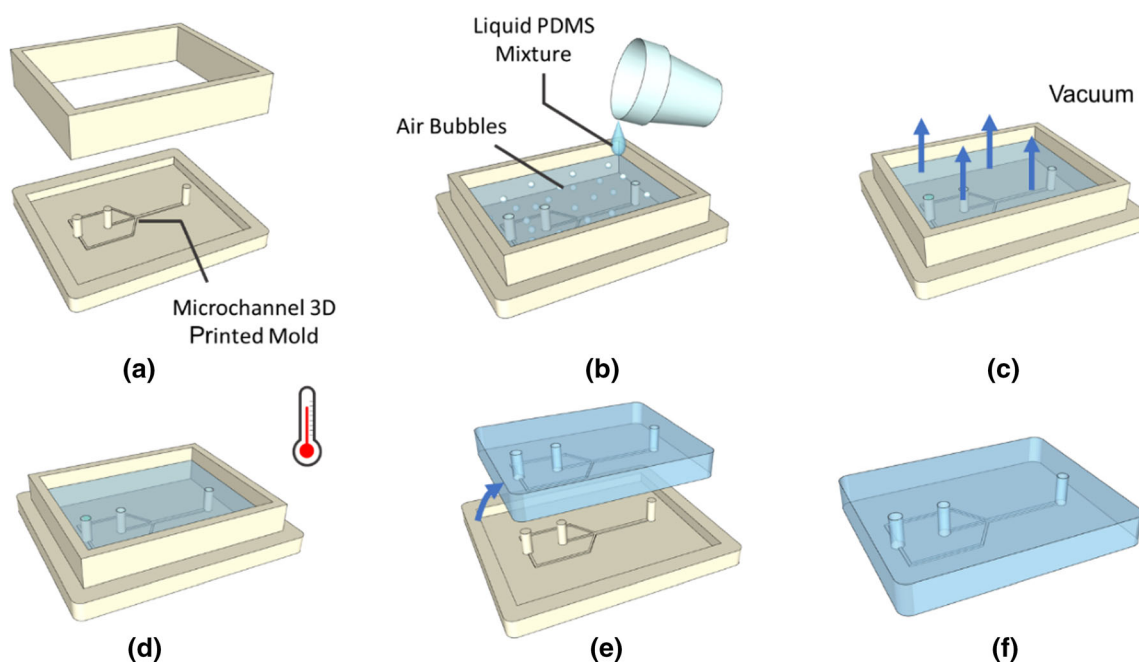
Before pouring into the 3D printing master mold, a PDMS prepolymer and a curing agent (Sylgard-184 Silicone Elastomer Kit, Dow Corning, Midland, MI, USA) were combined at a weight ratio of 10:1 and carefully stirred. After degassing the PDMS mixture until there were no bubbles on the surface, it was baked at 80 °C for at least 6 h. After cooling to room temperature, it was removed from the 3D printing mold. A successfully fabricated microchannel substrate is depicted in Fig. 6. In compared to photolithography, the whole manufacturing process takes less than 24 h, which is a considerable reduction in the time necessary to build a functioning prototype of a microfluidic structure. Some advantages of the disclosed technique are low cost, rapid prototyping, ease of design, direct molding and sealing of devices, masters mold reusable, and the ability to create complicated 3D systems.

2.3 Differential capacitive sensor fabrication based on PCB technology

The differential capacitive sensor was realized based on the standard FR4 printed circuit board fabrication process. Figure 7a shows a typical microfluidic sensing structure with a pair of coplanar electrodes used as the capacitive sensor. The electrodes are covered by a dielectric layer with a relative permittivity of ϵ_r . In this study, coplanar sensing electrodes were utilized to create an impedance sensing structure that consists of three copper electrodes Fig. 7b. The middle electrode was used as an exciting electrode, where the excitation signal is fed. The other two side-electrodes were utilized as the sensing electrodes in which voltage signal is picked up to the peripheral signal processing circuit.

Table 1 Characteristics of 3D printer materials

Property	VeroClear RGD810	VeroBlue RGD840	Rigur RGD450	Units
Tensile strength	50–65	50–60	40–45	MPa
Elongation at break	10–25	15–25	20–35	%
Modulus of elasticity	2000–3000	2000–3000	1700–2100	MPa
Flexural strength	75–110	60–70	52–59	MPa
Flexural modulus	2200–3200	1900–2500	1500–1700	MPa
Water absorption	1.1–1.5	1.5–2.2	–	%

**Fig. 4** 3D printed master molds made from **a** Rigur RGD450, **b** VeroBlue RGD840, and **c** VeroClear RGD810**Fig. 5** Microfluidic chip fabrication process based on the proposed rapid prototyping technique: **a** 3D-printed master mold preparation, **b** PDMS mixture casting, **c** degassing, **d** baking, **e** demolding, **f** created PDMS channel

In this study, coplanar micro-electrodes were created by patterning the copper layer on the FR4 substrate. Dimensions of the sensing structure are shown in Fig. 7b. CAD software was used to design the microelectrode structure, and the ink mask layer was patterned on the copper layer.

The substrate was then immersed in the FeCl_3 solution. The solution was used to expose the uncovered portion of the copper layer which was then removed from the FR4 substrate. The sandpaper was gently used to remove the remaining ink layer gently (Figs. 8a–d).

Fig. 6 Fabricated PDMS microchannel substrate. PDMS casted master mold **a** before, **b** after degasification, **c** a fabricated PDMS Y-junction and microchannel

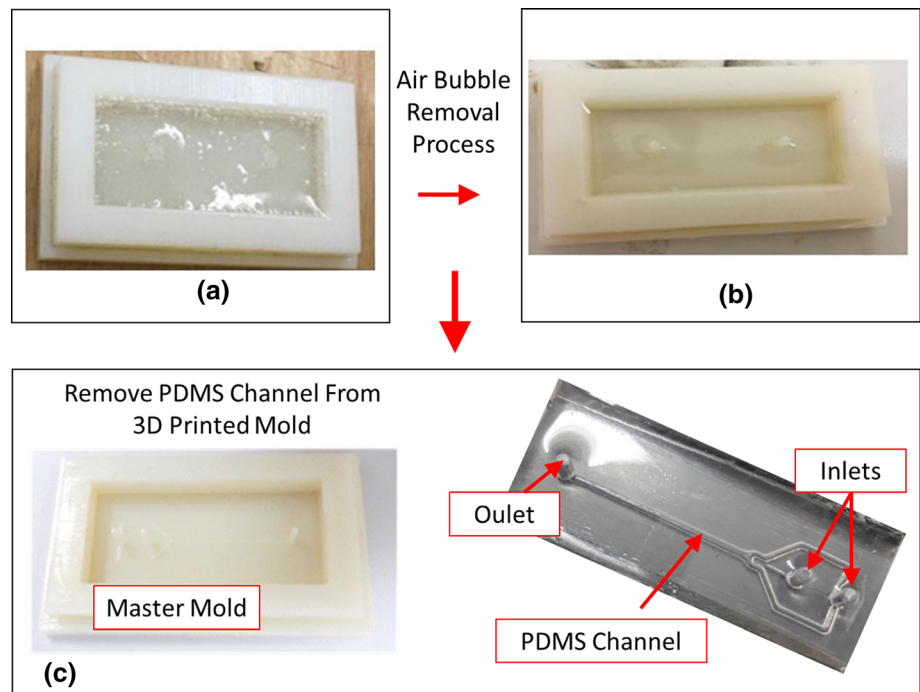
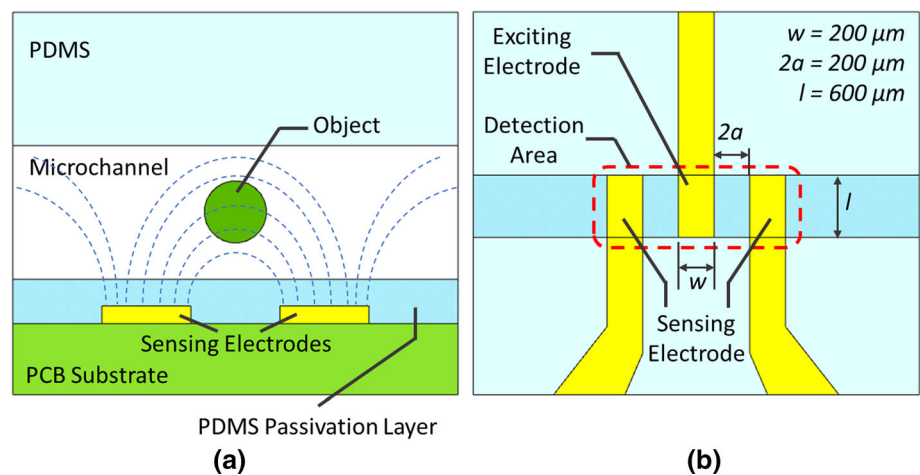


Fig. 7 Coplanar capacitive sensor design: **a** illustration of capacitance form by coplanar electrodes, **b** schematic of the three electrodes differential capacitive sensor



2.4 Integration of PDMS microchannel with the PCB platform

Figure 9 shows the integration process of PDMS microchannel with the PCB platform. A thin layer of PDMS is spin-coated on the electrode side of the fabricated FR4 PCB board (Fig. 10a). This thin layer will provide not only a flat surface that facilitates bonding with the PDMS structure but also create an insulating layer to avoid direct contact between the sensing electrodes and the solution in the microchannel. The thickness of the PDMS layer mainly depends on spinning speed and duration. In this study, we created a 30–100 μm thick layer of PDMS by spinning the PDMS mixture in the 30 s at the speed of 800–1000 rpm. Other factors that require attention are the type of PDMS,

and the ratio of curing agent and PDMS which are considered during experiments.

A PDMS prepolymer and a curing agent (Sylgard-184 Silicone Elastomer Kit, Dow Corning, Midland, MI, USA) were first mixed at a weight ratio of 10:1 and stirred thoroughly before being degassed in the vacuum chamber for 45 min. The output material was then spin-coated on the sensor-integrated side of the PCB board. A picture of the spin-coated PDMS layer on the FR4 board surface is shown in Fig. 10b. After coating, the Y-junction PDMS microchannel structure was aligned on the PCB board as described in the previous section and left on a hot plate for 2 h for mixture curing. Figure 10c shows the alignment of the capacitive sensor and the PDMS microchannel. The spin-coated liquid-PDMS layer was employed as an

Fig. 8 Coplanar capacitive sensor creation based on Printed Circuit Board Technology: **a** copper-FR4 substrate preparation, **b** ink-mask patterning, **c** copper etching, **d** coplanar capacitive sensor formation

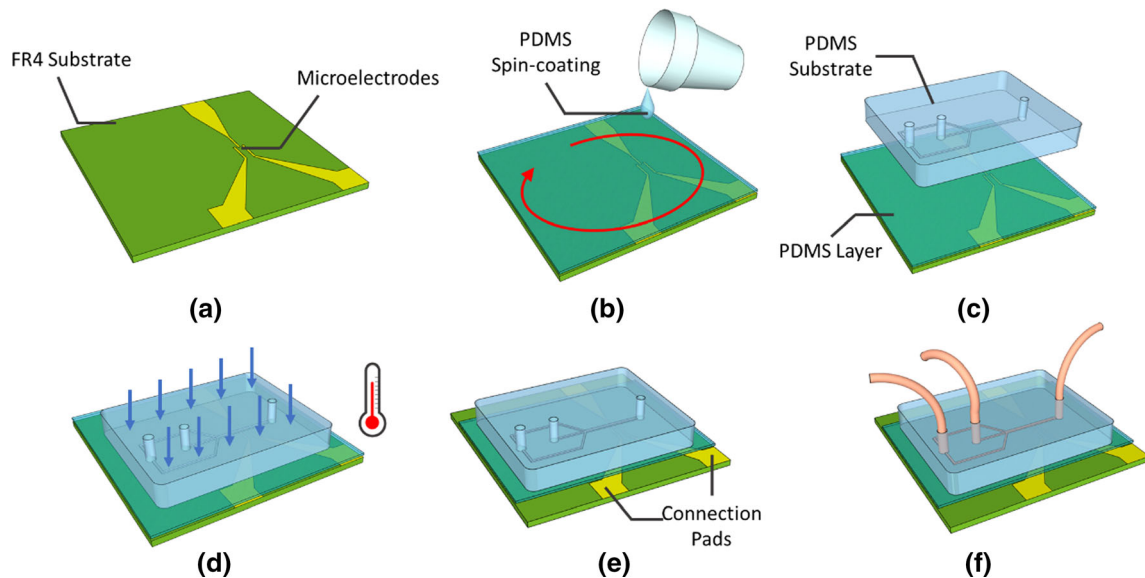
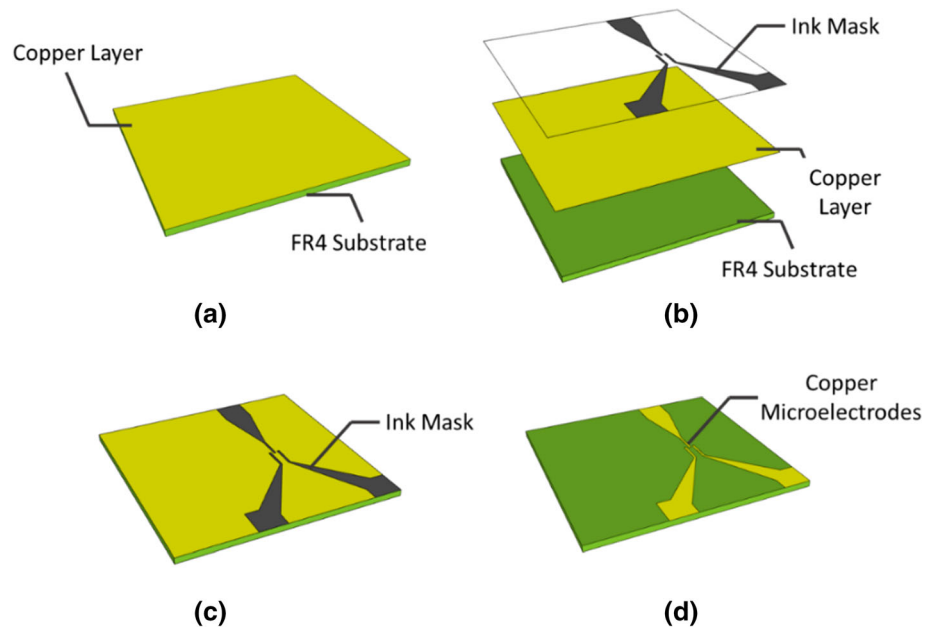


Fig. 9 Bonding the PDMS microchannel with the PCB platform process: **a** PCB with microelectrode patterned preparation, **b** adhesive layer coating, **c** alignment and placement of PDMS microchannel

substrate on PCB platform with microelectrodes, **d** baking, **e** PDMS layer at connection pads removal, **f** fabricated microfluidic chip with inlet/outlet

adhesive layer for sealing the microchannel with the sensing microelectrode structure. The sensor structure was aligned on the microchannel so that the electrodes were perpendicular to the microchannel, and the flow passed through the detection area. When a defect in the flow or an object moves along the microchannel and passes over the sensing area, the medium between electrodes is changed, causing impedance unbalance between the sensing electrodes. Hence, the capacitive sensor structure can provide a way to detect anomalies or two-phase flow in a microfluidic channel.

2.5 Experimental setup for validating the performance of the fabricated device

In this study, the microfluidic chip's functionality and performance were investigated to generate a two-phase flow, including air bubbles and water in the microfluidic channel. An integrated differential capacitive sensor was successfully fabricated and employed to detect the presence of air bubbles inside the fluidic flow. The

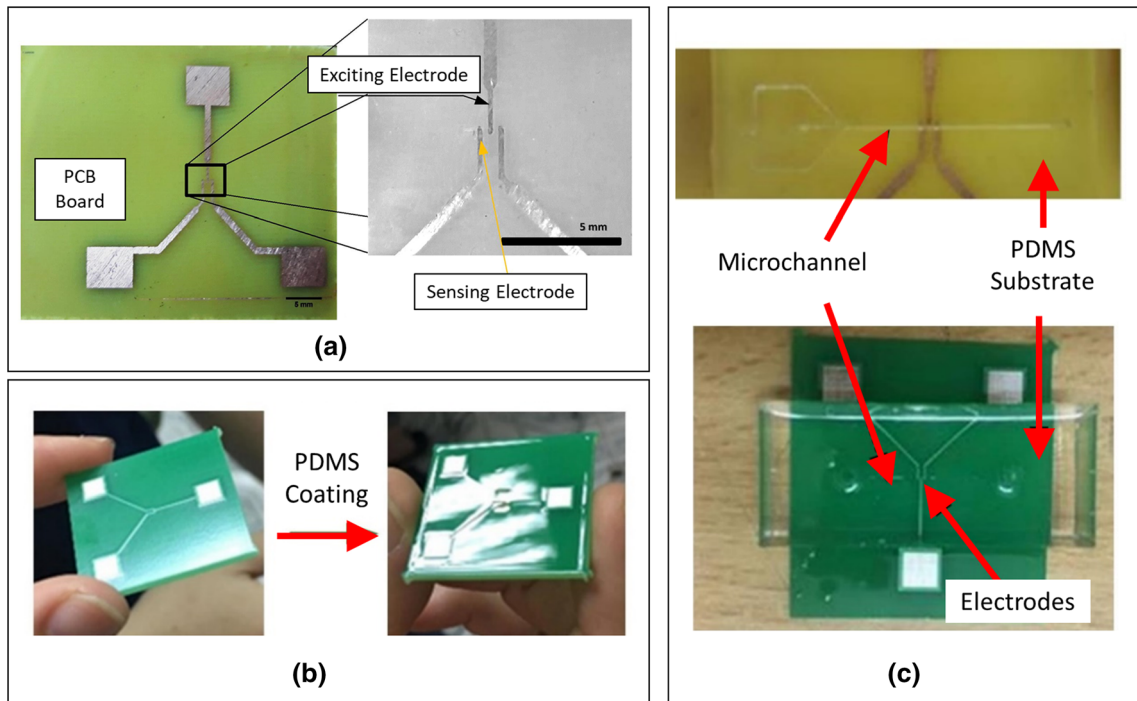
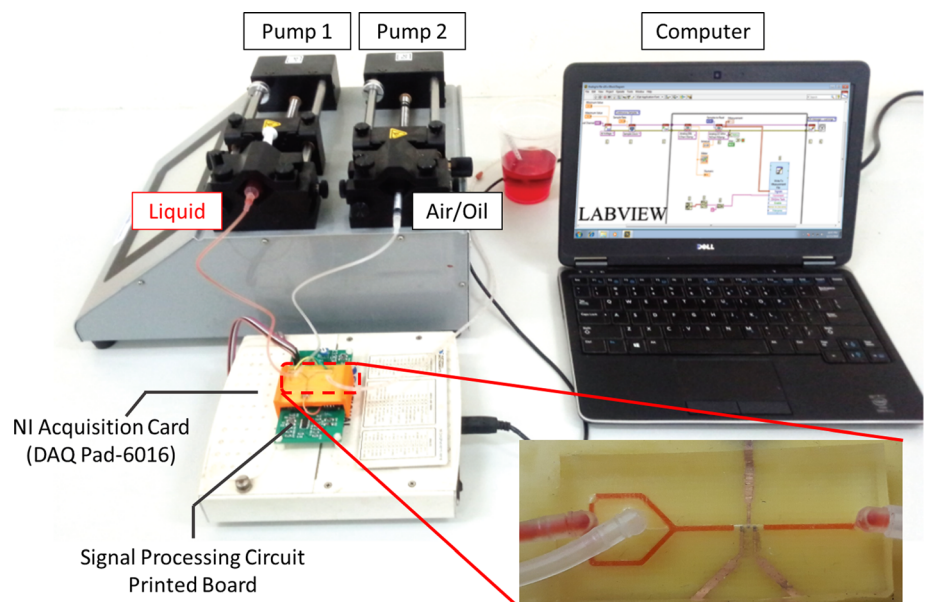


Fig. 10 Fabrication results: **a** the tri-electrode capacitive sensor fabricated on a PCB board, **b** fabricated PCB sensor before and after PDMS coating, **c** fabricated lab-on-PCB microfluidic chip after bonding with the single-channel and Y-junction channels

experimental setup is shown in Fig. 11. A dual syringe pump (Gemini 88, KD Scientific) is adopted to inject fluidic flows into the microfluidic channel inlets. The Y-shaped primary channel inlet is supplied with colored water, while air is supplied to the secondary channel inlet. At the Y-junction, airflow was squeezed into the water flow to create a two-phase flow in the microchannel outlet. In this experiment, a two-phase flow is generated by

employing two individual syringe pumps. By controlling the flow rate between two inlets of the microfluidic channel, the velocity and the volume of the air bubble in water flow could be investigated utilizing the differential capacitive sensor. The signal processing circuit supplied an alternating signal to the exciting electrode and acquired the sensing signal from sensing electrodes. A typical differential signal processing circuit was employed in this study

Fig. 11 Experiment setup with two syringes pumps to supply liquid and air/oil to the microchannels. The two-phase flow is achieved by the Y-junction microfluidic channel and can be detected by the integrated capacitive sensor



by using a high-speed instrumentation amplifier (INA111, Texas Instruments) followed by a high-precision balanced modulator/demodulator IC chip (AD630, Analog Devices) in the lock-in amplifier configuration to eliminate common noise and unwanted background signals. The output signal of the measurement circuit was acquired by an acquisition card (DAQ Pad-6016, NI), and the data was transferred to a computer through the LabVIEW interface for analysis, display, and storage.

3 Results and discussions

A microelectrode structure was successfully patterned and fabricated by the standard FR4 printed circuit board fabrication process. In order to integrate the microfluidic chip into the electrode sensor base, the mating of the PDMS substrate with the FR4 PCB substrate was done manually while the PDMS mixture was still liquid on the FR4 PCB substrate. During the process of joining two fabricated substrates, a small amount of uncured PDMS adhesive layer might be leaked into the microchannel structure. As a result, the channel may be damaged as PDMS remnants or channel distortion during the curing period. The most typical issue with this manufacturing method is channel obstruction. This insecurity impedes the chip creation process's success rate. Several master mold designs were successfully constructed and 3-D printed with varying dimension parameters, including Y-shaped channel and single-channel structure, to examine the manufacturing process's possibility and feasibility. Following the bonding procedure, water was progressively injected into the microfluidic to determine the success rate of the created microfluidic channel. The fabrication's success rate is shown in Tables 2 and 3. The bonding process of the PDMS microchannel with the FR4 PCB substrate was implemented manually while the PDMS mixture was still a liquid layer on the FR4 PCB substrate. As a result, the channel may be damaged due to remnant PDMS material or channel deformation during the curing process. This instability hinders the success rate of the chip fabrication process. It can be seen that the highest success rate was

Table 2 Fabrication success rate for single-channel chip

Channel's height and width (μm)	Success rate (%)
80×80	0
100×100	50
200×200	80

Table 3 Fabrication success rate for Y-channel chip

Single and Y Channel width (μm)	Success rate (%)
(100, 500)	20
(100, 600)	28
(100, 800)	43
(200, 500)	60
(200, 600)	71
(200, 800)	80

obtained at 80% according to the case of 200 μm single channel and 800–200 μm Y-Channel, respectively. Besides, it can be concluded that the current process can produce channels down to 100- μm -wide at a 50% success rate.

In order to fabricate smaller channels, fabrication processes and methods should be improved. The single-channel chip can be fabricated with a higher success rate than the multi-channel chip constructed by the more complicated structure. For example, the success rate reaches 50% with the 100 μm single-channel fabrication but only 20%, 28%, and 43% with the Y-channels of (100 μm , 500 μm), (100 μm , 600 μm), and (100 μm , 800 μm), respectively. The experimental findings reveal that the fabrication success rate is around 80% according to the 200- μm -in-dimension channel. Due to the printing technology and the suggested bonding procedure, a single channel with a dimension of 80 μm is not viable. The majority of the 200- μm -in-dimension channels were successfully manufactured. The 100- μm -in-dimension channel is useful, but further work is needed to enhance the procedure. Fabrication procedures and methods must be developed and optimized in order to produce narrower channels. The single-channel construction was more successful than the Y-shaped channel created by the more sophisticated arrangement. It can be seen that the more complicated the structure, the more difficult the fabrication. The suggested technique has the advantages of being simple, equipment-free, and time-saving, and it does not require any complicated facilities or equipment. In the future, the study of the deficiency and performance enhancement for the smaller complicated structure will be investigated.

One of the main limitations around the 3D-printing PDMS master mold is the roughness of the surfaces caused by deposition occurring in the finite strata in 2 axes. Figure 12 shows the structures of 300- μm -wide PDMS microchannel with the gradual channel wall transition in

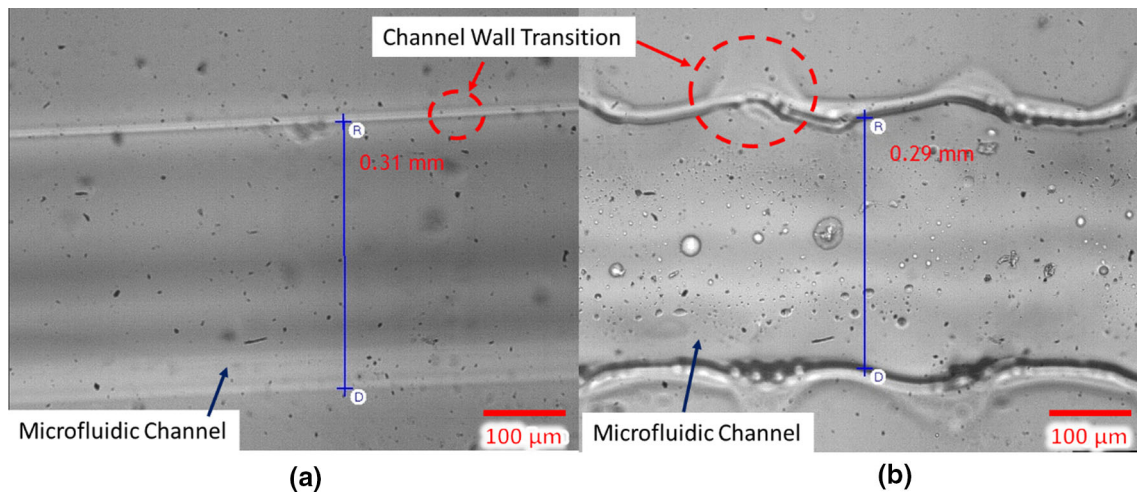


Fig. 12 Microscope image of a fabricated microfluidic channel utilizing 3D printed mold with: **a** a parallel ridge; and **b** perpendicular ridge to microchannel flow

case of the ridges of 3D printed mold is realized as parallel (Fig. 12a) and perpendicular (Fig. 12b) to the microfluidic channel flow. The movement direction of the nozzles and the roller during the printing process made the different patterns of these ridges. As can be seen in Fig. 12b, the perpendicular ridges to the microchannel flow of the master mold create the non-uniform of the lower edge of the channel formed by the channel wall and the substrate. This edge generates areas of the low fluidic flow where particles and fluid stagnate and become permanently stuck, resulting in the channel’s contamination and fouling. Therefore, to fabricate the single straight fluidic channel structures, it is highly recommended to orientate the movement direction of nozzles parallel to the microfluidic flow

The combination of 3D printing and PCB technology devices was examined using the microdroplet generation application to confirm the working operation. Two individual syringe pumps were used to produce a two-phase flow of oil and dye water in the microfluidic channel to highlight the chip’s operating capability to generate in-flow microdroplets. In this experiment, a fabricated microfluidic chip with a Y-channel junction was used. The successfully fabricated microfluidic device, which consists of a Y-junction 3D channel based on the PCB fabrication and 3D printing technologies, can create varied sizes of droplets. The flow rate of dye water was maintained at 20 μL/min, while the oil flow rate was alternated. Figure 13 depicts that the decrease of the oil pump flow rate caused the increase of the droplet’s size using the constructed chip. The size of the droplet may be regulated by controlling the flow rates of the liquid supplied into the two microfluidic channels. A camera microscope was used to capture the creation of the droplets and calculate the volume of

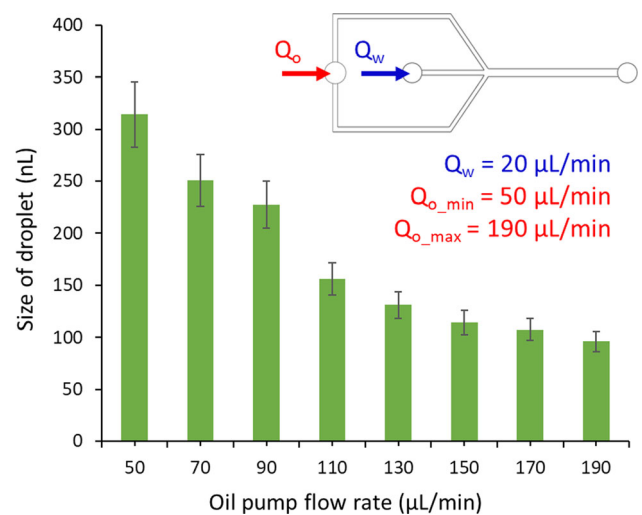


Fig. 13 Different sizes of droplets generated by changing the oil flow rate

generated microdroplets moving through the main channel. As shown in Fig. 13, the size of the droplet varies from less than around 100 nL to more than 310 nL according to the oil flow rate increases from 50 to 190 μL/min. The smaller droplets become as the oil flow rate increases.

Aside from that, the experiments were implemented to study the ability of on-chip generated microdroplet detection using the differential capacitive sensor on a PCB substrate. Figure 14 presents the respective signal obtained corresponding to the droplets generated. The inset depicts the microdroplet generation function of a Y-channel prototype. The movement of the microdroplet through the sensing area produces a peak signal by changing the differential impedance between the sensing electrode pairs. In particular, the acquired voltage signal shows the

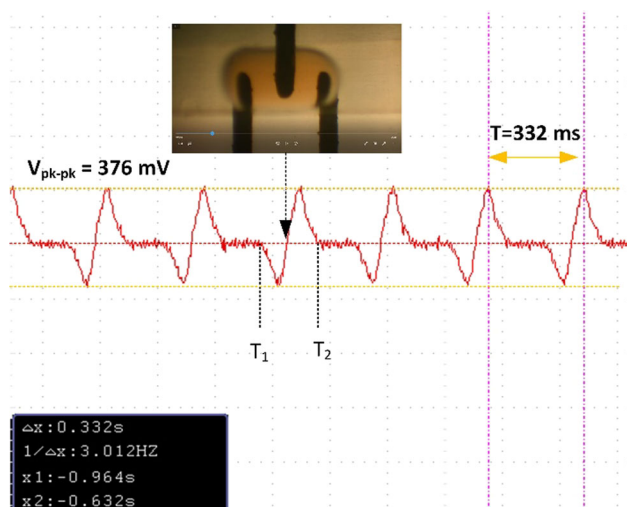


Fig. 14 Signal obtained corresponding to the droplets generated by dyed water (flow rate of 50 $\mu\text{L}/\text{min}$) and oil (flow rate of 110 $\mu\text{L}/\text{min}$)

consecutive bipolar pulses generated by the microdroplet passage across the detecting region at a water flow rate of 50 $\mu\text{L}/\text{min}$ and oil flow rate of 110 $\mu\text{L}/\text{min}$. The bipolar electrical voltage pulses were produced by the differential signal of two unipolar pulses according to the impedance change of each sensing electrode pair caused by the passage of a strange microdroplet over the sensing area. The red horizontal baseline shows the offset amplitude of the measuring circuit. The position of T_1 and T_2 shows the points at which the air bubble enters or departs the detecting zone. The microdroplet's velocity can be estimated by analyzing the time difference between T_1 and T_2 .

The preliminary experimental results also confirmed the procedure's practicality. Although there are still limitations of the success rate for microchannel structure being under 100- μm -in-dimension, this study verifies the effectiveness and feasibility of the application of the proposed RPT method to fabricate microfluidic systems. Meanwhile, this research work expands the application fields of RPT using 3D printing coupled with PCB manufacturing technique and lays a good foundation for future research work in lab-on-PCB microfluidic devices

4 Conclusions

In this study, a durable and adaptable approach for creating the microfluidic platform using the rapid prototyping technique based on PolyJet 3D technology and PCB manufacturing technology was proposed, implemented, and experimentally validated. The proposed fabrication method showed several advantages including fewer strict standards, ease of fabrication, shorter manufacturing time, and lower cost. The influence of numerous factors on the

method's performance was discussed and investigated. The experimental results show that the larger the channel's height, the more successful the fabrication, i.e., 80% of success rate for 200- μm -in-dimension channel. A microdroplet generation and detection system were demonstrated using the proposed fabrication process. The fabricated microfluidic device was confirmed to generate microdroplets using the flow-focusing approach with droplet volume ranging from 100 to 310 μL , and these droplets can be detected by impedance sensor structure. The acquired experimental results verify the possibility and feasibility of the proposed RPT method and lay a good foundation for future research work. This approach might serve as a platform technology, allowing the portable microfluidic platform created in lab-on-a-chip (LoC) systems, particularly for biomedical analytical applications.

Acknowledgements This research is funded by Vietnam National Foundation for Science and Technology Development (NAFOSTED) under grant number 103.99-2020.40. We would like to thank Mr. Du Tri Quang, Faculty of Physics, VNU University of Science, Hanoi, and Mr. Dau Hong Quan, VNU University of Engineering and Technology, for their assistance in chip packaging and experiments. Hang Tran Thanh was funded by Vingroup JSC and supported by the Master Scholarship Programme of Vingroup Innovation Foundation (VINIF), Institute of Big Data, code VINIF.2021.ThS.84.

References

- Anon 2019 is the datasheet of SUP706/SUP706B support material. The reference can be used as: Stratasy, BP_PJ_SUP706-706B Support Material_Application Note_A4_1219a, DOC-08423 Rev D
- Ashraf S, Aslam Z, Saleem S, Afnan S, Aamer M (2020a) Multi-biometric sustainable approach for human appellative. *CRPASE Trans Electr Electron Comput Eng* 06(03):146–152
- Ashraf S, Muhammad D, Shuaeeb M, Aslam Z (2020b) Development of Shrewd cosmetology model through fuzzy logic. *J Res Eng Appl Sci* 5(3):93–99
- Ashraf S, Saleem S, Ahmed T, Aslam Z, Muhammad D (2020c) Conversion of adverse data corpus to Shrewd output using sampling metrics. *Vis Comput Ind Biomed Art* 3(1):19
- Au AK, Bhattacharjee N, Horowitz LF, Chang TC, Albert Folch (2015) 3D-printed microfluidic automation. *Lab Chip* 15(8):1934–1941
- Bandyopadhyay A, Heer B (2018) Additive manufacturing of multi-material structures. *Mater Sci Eng R Rep* 129:1–16
- Bass L, Meisel NA, Williams CB (2016) Exploring variability of orientation and aging effects in material properties of multi-material jetting parts. *Rapid Prototyp J* 22(5):826–834
- Bishop GW (2016) 3D printed microfluidic devices. *Microfluidics for biologists: fundamentals and applications*. Springer, pp 103–13
- Bonyár A, Sántha R, Ring B, Varga M, Kovács JG, Harsányi G (2010) 3D rapid prototyping technology (RPT) as a powerful tool in microfluidic development. *Proc Eng* 5:291–94
- Cazón A, Morer P, Matey L (2014) PolyJet technology for product prototyping: tensile strength and surface roughness properties. *Proc Inst Mech Eng Part B J Eng Manuf* 228(12):1664–75

- Chen QL, Liu Z, Shum HC (2014) Three-dimensional printing-based electro-millifluidic devices for fabricating multi-compartment particles. *Biomicrofluidics* 8(6):064112
- Chen C, Mehl BT, Munshi AS, Townsend AD, Spence DM, Martin RS (2016) 3D-printed microfluidic devices: fabrication, advantages and limitations—mini review. *Anal Methods* 8(31):6005–6012
- Comina G, Suska A, Filippini D (2014) PDMS lab-on-a-chip fabrication using 3D printed templates. *Lab Chip* 14(2):424–430
- del Campo A, Greiner C (2007) SU-8: a photoresist for high-aspect-ratio and 3D submicron lithography. *J Micromech Microeng* 17(6):R81–95
- Donvito L, Galluccio L, Lombardo A, Morabito G, Nicolosi A, Reno M (2015) Experimental validation of a simple, low-cost, T-junction droplet generator fabricated through 3D printing. *J Micromech Microeng* 25(3):35013
- Han W, Chen X (2020) A review: applications of ion transport in micro-nanofluidic systems based on ion concentration polarization. *J Chem Technol Biotechnol* 95(6):1622–1631
- Kise DP, Reddish MJ, Dyer RB (2015) Sandwich-format 3D printed microfluidic mixers: a flexible platform for multi-probe analysis. *J Micromech Microeng* 25(12):124002
- Kontakis K, Petropoulos A, Kaltsas G, Speliotis T, Gogolides E (2009) A novel microfluidic integration technology for PCB-based devices: application to microflow sensing. *Microelectron Eng* 86(4–6):1382–1384
- Li J, Ge J, Yin Y (2008) Multiplexed affinity-based protein complex purification. *Anal Chem* 80(18):7068–7074
- Liu RH, Grodzinski P, Yang J, Lenigk R (2008) Self-contained, fully integrated biochips for sample preparation, PCR amplification and DNA microarray analysis. *Integr Biochips DNA Anal* 76(7):46–67
- Lv H, Chen X (2021) New insights into the mechanism of fluid mixing in the micromixer based on alternating current electric heating with film heaters. *Int J Heat Mass Transf* 181:121902
- Lv H, Chen X, Xiangwei Z (2021) Optimization of micromixer with cantor fractal baffle based on simulated annealing algorithm. *Chaos Solitons Fractals* 148:111048
- Lv H, Chen X, Wang X, Zeng X, Ma Y (2022) A novel study on a micromixer with cantor fractal obstacle through grey relational analysis. *Int J Heat Mass Transf* 183:122159
- Marshall LA, Wu LL, Babikian S, Bachman M, Santiago JG (2012) Integrated printed circuit board device for cell lysis and nucleic acid extraction. *Anal Chem* 84(21):9640–9645. <https://doi.org/10.1021/ac302622v>
- McDonald JC, Whitesides GM (2002) Poly(dimethylsiloxane) as a material for fabricating microfluidic devices. *Acc Chem Res* 35(7):491–499
- McDonald JC, Duffy DC, Anderson JR, Chiu DT, Wu H, Schueller OJ, Schueller, Whitesides GM (2000) Fabrication of microfluidic systems in poly(dimethylsiloxane). *Electrophoresis* 21(1):27–40
- Moschou D, Tserepi A (2017) The lab-on-PCB approach: tackling the MTAS commercial upscaling bottleneck. *Lab Chip* 17(8):1388–1405
- Pinto VC, Sousa PJ, Cardoso VF, Minas G (2014) Optimized SU-8 processing for low-cost microstructures fabrication without cleanroom facilities. *Micromachines* 5(3):738–55
- Quang LD, Quoc TV, Nhu CN, Thu HN, Thanh HT (2019) Development of a flow focusing droplet generation microfluidic system based on rapid prototyping technique. In: The 7th international workshop on nanotechnology and application—IWNA 2019. Phan Thiet, Vietnam, pp 327–31
- Quang LD, Bui TT, Hoang B-A, Nhu CN, Thuy HTT, Jen C-P, Duc TC (2020) Biological living cell in-flow detection based on microfluidic chip and compact signal processing circuit. *IEEE Trans Biomed Circuits Syst* 14(6):1371–1380
- Rahman Md, Rebrov E (2014) Microreactors for gold nanoparticles synthesis: from Faraday to flow. *Processes* 2(2):466–493
- Rapp BE, Gruhl FJ, Länge K (2010) Biosensors with label-free detection designed for diagnostic applications. *Anal Bioanal Chem* 398(6):2403–2412
- Sánchez JL, Acer. OYF, Henry H, Joda B, Werne Solnestam L, Kvastad E, Johansson P, Akan J, Lundeborg N, Lladach D, Ramakrishnan I, Riley, O’Sullivan CK (2016) Multiplex PCB-based electrochemical detection of cancer biomarkers using MLPA-barcode approach. *Biosens Bioelectron* 82:224–232
- Scott SM, Ali Z (2021) Fabrication methods for microfluidic devices: an overview. *Micromachines* 12(3):319
- Tran TH, Do QL, Hoang BA, Bui TT, Chu DT, Jen C-P (2021) A serpentine microchannel with added cavities platform for magnetic separation of lung adenocarcinoma cells utilizing aptamer-conjugated magnetic bead approach. In: The 21st international conference on solid-state sensors, actuators and microsystems, 20–25 June 2021, pp 992–95
- Vu IQ, Bass LB, Williams CB, Dillard DA (2018) Characterizing the effect of print orientation on interface integrity of multi-material jetting additive manufacturing. *Addit Manuf* 22:447–461
- Vu I, Bass L, Meisel N, Orler B, Williams CB, Dillard DA (2020) Characterization of multi-material interfaces in polyjet additive manufacturing. In: Proceedings—26th annual international solid freeform fabrication symposium—an additive manufacturing conference, SFF 2015 959–82
- Vu-Dinh H, Quang LD, Chang CC, Chun-Ping J (2021) Immunomagnetic separation in a novel cavity-added serpentine microchannel structure for the selective isolation of lung adenocarcinoma cells. *Biomed Microdevices* 23(4):51
- Waheed S, Cabot JM, Macdonald NP, Lewis T, Guijt RM, Paull B, Breadmore MC (2016) 3D printed microfluidic devices: enablers and barriers. *Lab Chip* 16(11):1993–2013
- Walczak R, Adamski K (2015) *J Micromech Microeng* 25:085013. <https://doi.org/10.1088/0960-1317/25/8/085013>
- Yang H, Lim JC, Liu Y, Qi X, Yap YL, Dikshit V, Yeong WY, Wei J (2017) Performance evaluation of proJet multi-material jetting 3D printer. *Virtual Phys Prototyping* 12(1):95–103

Publisher's note Springer Nature remains neutral with regard to jurisdictional claims in published maps and institutional affiliations.